

Transient chaos in two coupled, dissipatively perturbed Hamiltonian Duffing oscillators

S. Sabarathinam^a, K. Thamilaran^a, L. Borkowski^b, P. Perlikowski^{b,*}, P. Brzeski^b, A. Stefanski^b, T. Kapitaniak^b

**przemyslaw.perlikowski@p.lodz.pl*

^a*Center for Nonlinear Dynamics, School of Physics, Bharathidasan University, Tiruchirappalli, India*

^b*Division of Dynamics, Lodz University of Technology, Stefanowskiego 1/15, 90-924 Lodz, Poland*

Abstract

The dynamics of two coupled, dissipatively perturbed, near-integrable Hamiltonian, double-well Duffing oscillators has been studied. We give numerical and experimental (circuit implementation) evidence that in the case of small positive or negative damping there exist two different types of transient chaos. After the decay of the transient chaos in the neighborhood of chaotic saddle we observe the transient chaos in the neighborhood of unstable tori. We argue that our results are robust and they exist in the wide range of system parameters.

Keywords: Duffing oscillators, Hamiltonian chaos, chaotic saddle, transient chaos, electrical circuits.

1. Introduction

Practical dynamical systems are mainly quasihyperbolic [1, 2], i.e., many different types of attractors co-exist in the phase space. In such systems we often observe the phenomenon of transient chaos [3, 4, 5, 6, 17], where for almost all initial conditions within some practically important range, the system trajectory evolves on a strange chaotic repeller (chaotic saddle) for significantly long period of time, t^* say, and afterward, for $t > t^*$, converges to the regular attractor. The value of t^* will of course vary from trajectory to trajectory, and may be very sensitive to the initial conditions, but representative average of t^* can be used to describe the phenomena of transient chaos. Transient chaos has been found to be a typical behavior in the dissipatively perturbed near Hamiltonian systems [4, 5, 6].

Our studies are devoted to the dynamics of two bi-directionally coupled conservative Duffing oscillators, i.e., the signal from first system is sent to second one and vice versa. This type of coupling is commonly met in all fields of science, i.e., biology [7, 8, 9], quantum systems [10, 11, 12, 13], lasers [14] ect. The single Duffing system is a model of pendulum, a neuronal groups or a Josephson-junction [18, 19, 20, 21]. When we introduce coupling between oscillators one can observe a functional relation between them [22]. Due to coupling, phase space is extended from two to four dimensions and additionally to periodic and quasiperiodic dynamics chaotic and hyperchaotic behavior can be observed [23, 24, 25]. The appearance of coupling causes energy transfer from one oscillator to another and one can observe behaviors like beating, synchronization, oscillation death, creation of spatiotemporal structures ect. [26, 27, 28, 29, 30, 31, 32]

In some cases the dynamics presented in numerical investigations is not confirmed in experiments due to the parameter mismatch introduced by real elements. This is the reason why we experimentally realized two coupled Duffing oscillators as an electronic circuit. Building of the experimental setup, consisting of two coupled Duffing oscillators, is relatively simple, but dynamics of this circuit is enough complicated to show a

*Corresponding author

Email address: przemyslaw.perlikowski@p.lodz.pl (P. Perlikowski)

complex behavior commonly met in quantum systems [30, 34, 35, 36] without dissipation and with small negative and positive damping. We investigate the properties of the experimentally observed quasiperiodic and chaotic trajectories. We show that when the near-integrable Hamiltonian system is perturbed by dissipation (positive or negative), then the stable orbits become simple attracting or repelling sinks, the Kolmogorov-Arnold-Moser tori are destroyed and persistent chaotic motion disappears. We give experimental evidence that in the perturbed system the chaotic saddle exists and is manifested by the transient chaotic behavior. After the decay of this transient chaos we observe the second type of transient chaos, i.e., unpredictable behavior in the neighborhoods of unstable tori. We show that the obtained results are robust and they exist for the wide range of system parameters and energy levels.

The paper is organized as follows. Sec. 2 describes the system under consideration. In Sec. 3 and 4 we present our results of stability analysis and numerical simulations. The comparison of numerical and experimental results is shown in Sec. 5. Finally, we conclude the paper in Sec. 6.

2. The model

2.1. Conservative system

As we mention before as a model of nonlinear system, we consider the Duffing oscillator [37]. This system is one of the typical and widely explored examples of non-linear oscillator. It is governed by the following dimensionless second-order differential equation

$$\frac{d^2 z}{d\tau^2} + \frac{dV(z)}{dz} = 0, \quad (1)$$

where z and $\frac{dz}{d\tau}$ is a position and velocity of the system, τ is the dimensionless time. Considered oscillator (1) is conservative and integrable. In our investigation we consider a double-well potential:

$$V(z) = -\frac{\alpha}{2}z^2 + \frac{\beta}{4}z^4, \quad (2)$$

so the system has one saddle and two non-hyperbolic centers.

The single Duffing system exhibits rich and baffling varieties of regular and chaotic motions. When two systems given by equation (1) are coupled, the dimension of phase space is extended to four and dynamics becomes even more complicated. In our investigations we consider a classical bi-directional linear coupling and identical systems (with exactly the same values of parameters). Basing on this assumptions one can write an expression of potential for two coupled Duffing oscillators:

$$V(z_1, z_2) = -\frac{\alpha}{2}z_1^2 + \frac{\beta}{4}z_1^4 - \frac{\alpha}{2}z_2^2 + \frac{\beta}{4}z_2^4 + \frac{k}{2}(z_1 - z_2)^2, \quad (3)$$

where subscript indicate system number (1 or 2) and k is the coupling parameter. The kinetic energy is given by following formula:

$$T(z_1, z_2) = \frac{1}{2} \left(\left(\frac{dz_1}{d\tau} \right)^2 + \left(\frac{dz_2}{d\tau} \right)^2 \right), \quad (4)$$

Formulas (3) and (4) allows to derive, using equations of Lagrange of second type, the following equations which describes the dynamics of coupled double-double wells Duffing oscillators,

$$\begin{aligned} \frac{d^2 z_1}{d\tau^2} - \alpha z_1 + \beta z_1^3 + k(z_2 - z_1) &= 0, \\ \frac{d^2 z_2}{d\tau^2} - \alpha z_2 + \beta z_2^3 + k(z_1 - z_2) &= 0, \end{aligned} \quad (5)$$

where $\alpha > 0$, $\beta > 0$ and $k > 0$.

2.2. Non-conservative system

When one considers system (5) with damping (positive or negative) the energy dissipated or supply? (added) to the oscillators is given by the Rayleigh term:

$$D(z_1, z_2) = b_1 \frac{1}{2} \left(\frac{dz_1}{d\tau} \right)^2 + b_2 \frac{1}{2} \left(\frac{dz_2}{d\tau} \right)^2, \quad (6)$$

where b_1 and b_2 are damping coefficients of first and second oscillator. In our work we consider identical systems, so $b_1 = b_2 = b$. Positive b implies positive damping hence the oscillations are damped out and system slowly diverges to one of the stable equilibrium position. In opposite case (negative damping) the energy is pumped to the system and trajectory escape to infinity. Equations of damped system have following form:

$$\begin{aligned} \frac{d^2 z_1}{d\tau^2} + b \frac{dz_1}{d\tau} - \alpha z_1 + \beta z_1^3 + k(z_2 - z_1) &= 0, \\ \frac{d^2 z_2}{d\tau^2} + b \frac{dz_2}{d\tau} - \alpha z_2 + \beta z_2^3 + k(z_1 - z_2) &= 0. \end{aligned} \quad (7)$$

3. Stability analyzis

To hold generality, we do the stability analyzis using equations with damping. System (7) can be rewrite as a four first order ODEs:

$$\begin{aligned} \frac{dx_1}{d\tau} &= x_2, \\ \frac{dx_2}{d\tau} &= -bx_2 + \alpha x_1 - \beta x_1^3 - k(x_1 - x_3), \\ \frac{dx_3}{d\tau} &= x_4, \\ \frac{dx_4}{d\tau} &= -bx_4 + \alpha x_3 - \beta x_3^3 - k(x_3 - x_1) = 0. \end{aligned} \quad (8)$$

where $x_1 = z_1$, $x_2 = \frac{dz_1}{d\tau}$, $x_3 = z_2$ and $x_4 = \frac{dz_2}{d\tau}$. Then we calculate the steady states of system (8), we obtain nine equilibrium positions. Due to symmetries only four of them are unique. To determinate their stability we linearized system 8 around arbitrary equilibrium $(x_{10}, x_{20}, x_{30}, x_{40})$:

$$\delta \dot{X} = \begin{bmatrix} -\lambda & 1 & 0 & 0 \\ \alpha - 3\beta x_{10}^2 - k & -b - \lambda & k & 0 \\ 0 & 0 & -\lambda & 1 \\ k & 0 & \alpha - 3\beta x_{30}^2 - k & -b - \lambda \end{bmatrix} \delta X \quad (9)$$

where $\delta X = [\delta x_1, \delta x_2, \delta x_3, \delta x_4]^T$. Solution of Eq. 9 in respect to λ gives us four eigenvalues for each steady state which govern its stability. We consider three cases of damping coefficient b values: conservative system ($b = 0.0$), positive ($b > 0$) and negative ($b < 0$) sign of damping. The eigenvalues (see Table 1) are calculated for following values of system parameters: $\beta = 0.85$, $\alpha = 0.3$ and $k = 0.08$.

Only in the case of positively damped system ($b = 0.0001$) we observe stable equilibrium No. 1 and 4 (see Table 1). The rest are unstable centers (No. 2, 3 and 5). For Hamiltonian system No. 1 and 4 become hyperbolic equilibrium with two pairs of complex conjugated eigenvalues on imaginary axis. Finally, for negative damping ($b = -0.0001$) all steady states are unstable. Their destabilization occurs trough the double Hopf bifurcation.

4. Numerical results

In this section we show numerical results concerning dynamics of Eqs (5) and (7). We consider three cases (similarity as for steady states): conservative and two others with small damping (positive or negative). Such an approach lets us to investigate behavior of considered system in details. In the conservative limit ($b = 0$) the dynamics of system (5) is dependent on initial conditions and the total energy of the system. The total energy of the Hamiltonian system (5), based on formulas (3,4), is equal to: $\mathcal{H} = T + V$. In our

No.	Steady state	Positive damping ($b = 0.0001$)	Ham. system ($b = 0.0$)	Negative damping ($b = -0.0001$)
1	$x_{10} = \pm 0.594$ $x_{30} = \pm 0.594$	$\lambda_{1,2} = -0.00005 \pm 0.87178i$ $\lambda_{3,4} = -0.00005 \pm 0.774597i$	$\lambda_{1,2} = \pm 0.87178i$ $\lambda_{3,4} = \pm 0.774597i$	$\lambda_{1,2} = 0.00005 \pm 0.87178i$ $\lambda_{3,4} = 0.00005 \pm 0.774597i$
2	$x_{10} = \pm 0.467$ $x_{30} = \mp 0.201$	$\lambda_1 = -0.360894$ $\lambda_{2,3} = -0.00005 \pm 0.591784i$ $\lambda_4 = 0.360794$	$\lambda_{1,2} = \pm 0.360844$ $\lambda_{3,4} = \pm 0.591784i$	$\lambda_1 = -0.360894$ $\lambda_{2,3} = 0.00005 \pm 0.591784i$ $\lambda_4 = 0.360794$
3	$x_{10} = \pm 0.201$ $x_{30} = \mp 0.467$	$\lambda_1 = -0.360894$ $\lambda_{2,3} = -0.00005 \pm 0.591784i$ $\lambda_4 = 0.360794$	$\lambda_{1,2} = \pm 0.360844$ $\lambda_{3,4} = \pm 0.591784i$	$\lambda_1 = -0.360894$ $\lambda_{2,3} = 0.00005 \pm 0.591784i$ $\lambda_4 = 0.360794$
4	$x_{10} = \pm 0.406$ $x_{30} = \mp 0.406$	$\lambda_{1,2} = -0.00005 \pm 0.34641i$ $\lambda_{3,4} = -0.00005 \pm 0.52915i$	$\lambda_{1,2} = \pm 0.34641i$ $\lambda_{3,4} = \pm 0.52915i$	$\lambda_{1,2} = 0.00005 \pm 0.34641i$ $\lambda_{3,4} = 0.00005 \pm 0.52915i$
5	$x_{10} = 0.0$ $x_{30} = 0.0$	$\lambda_1 = -0.547773$ $\lambda_2 = -0.374216$ $\lambda_3 = 0.374116$ $\lambda_4 = 0.547673$	$\lambda_{1,2} = \pm 0.547673$ $\lambda_{3,4} = \pm 0.374116$	$\lambda_1 = -0.547673$ $\lambda_2 = -0.374116$ $\lambda_3 = 0.374216$ $\lambda_4 = 0.547773$

Table 1: List of unique steady states and their stability for system 7 with $b = 0.0001$, $b = 0.0$ and $b = -0.0001$. equilibrium No 1 to 4 are symmetric and No. 5 is single. For all equilibrium $x_{20} = x_{40} = 0.0$.

numerical calculations we take the same values of parameters ($\beta = 0.85$, $\alpha = 0.3$, $k = 0.08$) as in steady state analysis.

In Figure 1(a-c) we plot the projections of Poincaré maps for three different energy levels. The reference values of total energy are following (i) $\mathcal{H} = 0.105156$ (Figure 1(a)), (ii) $\mathcal{H} = 0.167042$ (Figure 1(b)), (iii) $\mathcal{H} = 4.81512$ (Figure 1(c)). To plot Poincaré maps we consider from 400 up to 600 sets of initial conditions (for each level of energy). We randomly generate three initial values and calculate the last one ($\frac{dx_2(0)}{dt}$) assuming the constant level of energy \mathcal{H} - in some cases this fourth value is a complex number, so we neglect it and generate a new set of initial conditions. In all cases there is a persistent regular motion on some perturbed Kolmogorov-Arnold-Moser (KAM) orbits and on KAM "island" orbits in the phase space.

Regions of persistent chaotic motion are densely interwoven with regular regions. The measures of the regular and chaotic regions can vary widely, both within the phase plane and as a function of the system parameters and energy levels. More detailed analysis of the system (5), corresponding to the case shown in Figure 1(a) is presented in Figure 2(a-c). To identify the dynamics of system and its changes in time we calculate transient Lyapunov exponents [38]. For Hamiltonian systems sum of their spectrum is equal to zero, moreover we do not observe attractors, so the values of Lyapunov exponents inform us about the properties of given trajectory. In case of slightly damped systems, the change in spectrum of Lyapunov exponents let us predict the qualitative transition of system dynamics. In Figure 2(a) we show time series of $x_1(t)$, in Figure 2(b) four Lyapunov exponents and in last one (Figure 2(c)) the zoom of time series. One can see that after transient time the values of Lyapunov exponents stabilize with one positive, two zeros and one negative. Two zeros Lyapunov exponents come from the fact that one is connected with direction along the flow and the second one is due to the symmetry of the spectrum [38].

When near-integrable system (7) is perturbed by dissipation (positive: $b > 0$ or negative: $b < 0$), then the stable orbits become simple attracting ($b > 0$) or repelling ($b < 0$) sinks, the KAM tori are destroyed and replaced by unstable tori, so the persistent chaotic motion disappears. Instead of persistent chaos one can observe chaotic saddle. Chaotic saddle is a typical non-attracting chaotic set which repels trajectories only along some special hypersurface in the phase space (unstable manifold). Whereas, along other invariant hypersurface (stable manifold), the set can actually attract nearby trajectories. Transient chaos in systems described by differential equations is typically related to chaotic saddles [3, 4, 5, 6, 17]. During time evolution one can observe a convergence to one of the stable steady states (positive damping) or escape to infinity (negative damping).

Transient chaotic time series of Eq. (7) are shown in Figure 3(a-c) (positive damping $b = 0.0001$) and Figure 3(d-f) (negative damping $b = -0.0001$). We calculated time series for the following initial condition:

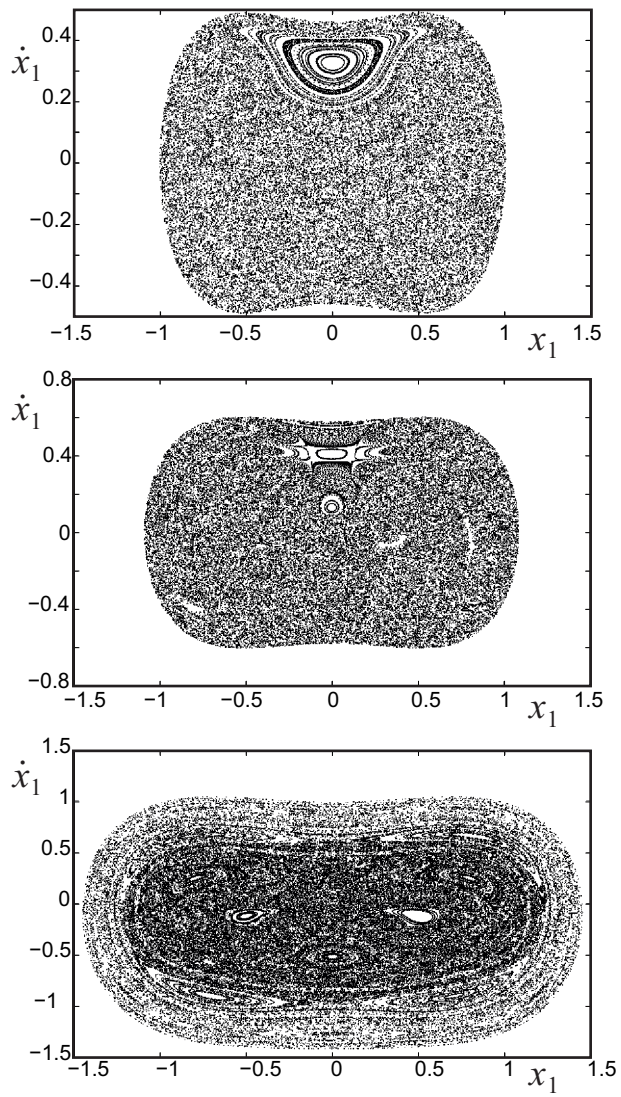


Figure 1: Poincaré maps of eq. (3) for three different energy spaces, $k = 0.08$; (a) $\mathcal{H} = 0.105156$, (b) $\mathcal{H} = 0.167042$, (c) $\mathcal{H} = 4.81512$.

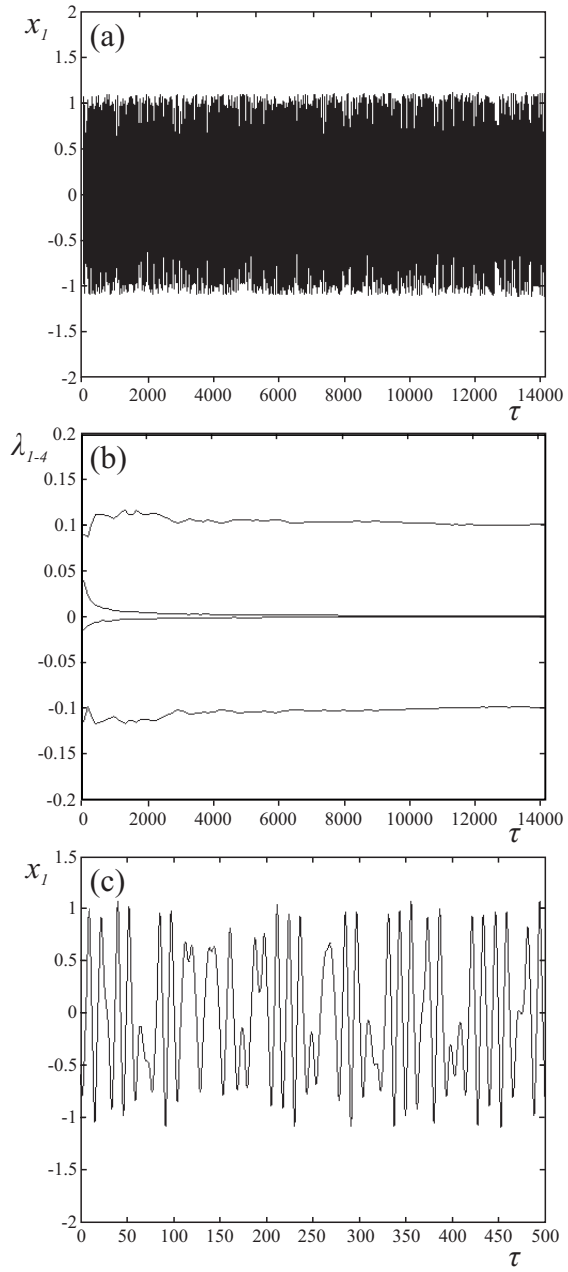


Figure 2: Time plots of conservative system (eqs (3)); (a) $x_1(\tau)$, (b) transient Lyapunov exponents, (c) enlargement of (a). Initial condition: $x_1(0) = -0.5021$, $\frac{dx_1(0)}{dt} = -0.17606$, $x_2(0) = -0.96946$, $\frac{dx_2(0)}{dt} = 0.34206$ and energy level $\mathcal{H} = 0.105156$.

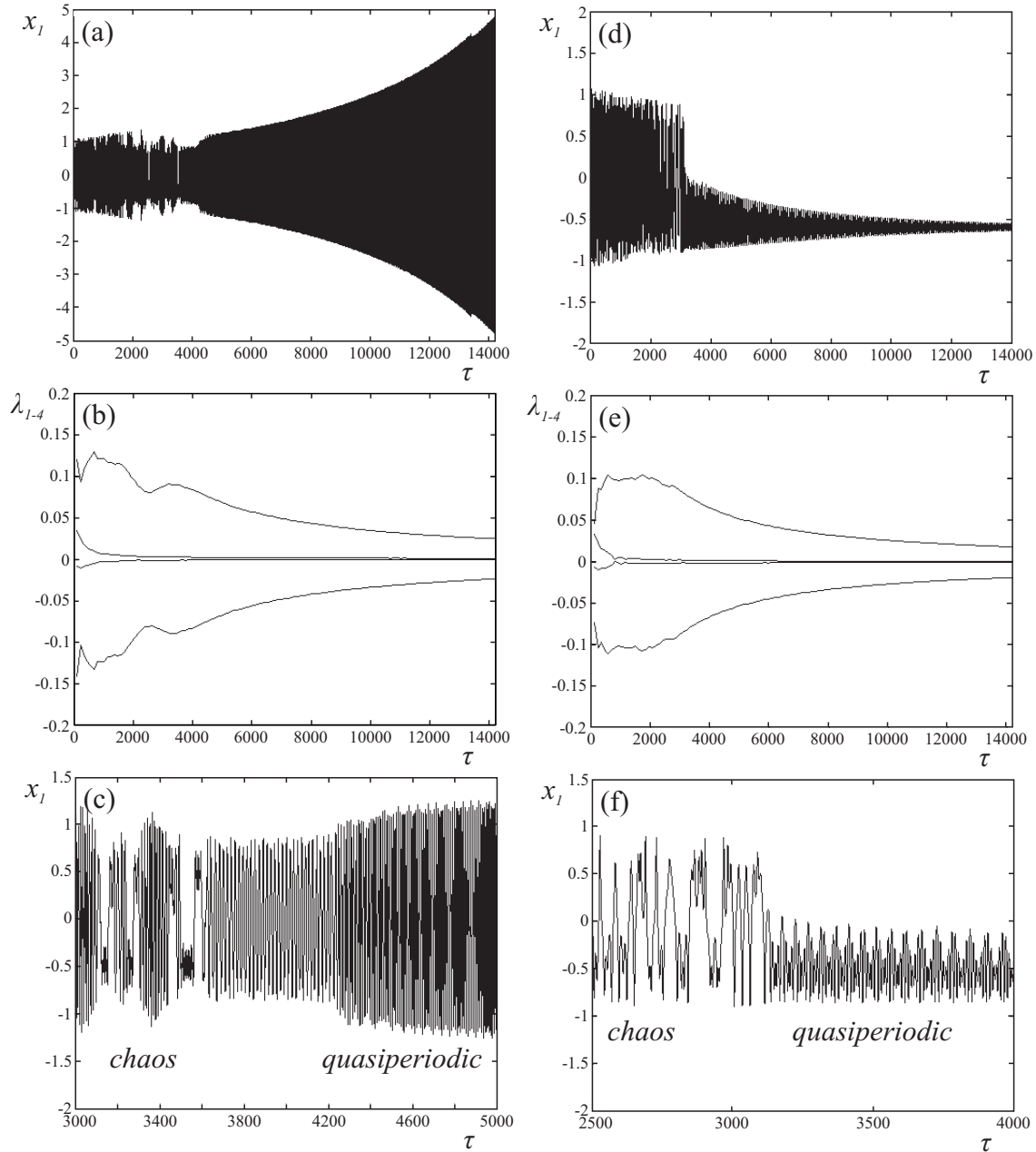


Figure 3: Time series of dissipatively perturbed Eq. (3) for negative damping $b = -0.0001$; (a) $x_1(\tau)$, (b) transient Lyapunov exponents, (c) enlargement of (a) and for positive damping $b = 0.0001$; (d) $x_1(\tau)$, (e) transient Lyapunov exponents, (f) enlargement of (d).

$x_1(0) = 0.5021$, $\frac{dx_1(0)}{d\tau} = 0.17606$, $x_2(0) = 0.96946$, $\frac{dx_2(0)}{d\tau} = 0.34206$. The time series in Figure 3(a) and Figure 3(d) exhibit the period of transient chaos in the neighborhood of chaotic saddle. At the end of this period the trajectory still has chaotic properties but evolves in the neighborhoods of the sequence of unstable tori with decreasing sizes and finally tends to one of the stable fixed points ($x_{10} = x_{30} = 0.594$, $x_{20} = x_{40} = 0.0$) or escape to infinity. Figure 3(b) and Figure 3(e) show the evolution of transient Lyapunov exponents. For small values of τ ($\tau < 0.6 \times 10^4$) two exponents are negative and two are positive. With the increase of τ ($\tau \in [0.6 \times 10^4, 3.4 \times 10^4]$) two Lyapunov exponents become zero and the other two (negative and positive) stabilize in the period of the evolution in the neighborhood of chaotic saddle. During the transient chaos in the neighborhood of unstable tori two of the Lyapunov exponents are positive and two are negative, but their absolute values slowly decrease. Finally the sum of all Lyapunov exponents becomes negative (positive damping) or positive (negative damping). The transition between transient chaos in the neighborhood of chaotic saddle and transient chaos in the neighborhood of unstable tori is presented at the enlargement in Figure 3(c) and Figure 3(f). The life time of the transient chaos exponentially decays with the increase of the absolute value of b .

5. Experimental results

Dynamical system (7) can be implemented as an electronic circuit shown in Figure 4(a,b). Figure 4(a) presents the circuit diagram and Figure 4(b) its laboratory realization. Each oscillator is shown in a black frame and is built using two capacitors, five resistors, and two multipliers AD-633, introducing nonlinearity. We measured the voltage at points $V_{1,2}$ and $\delta V_{1,2}$, which are related to $z_{1,2}$ and $\frac{dz_{1,2}}{dt}$, respectively. In order to set the initial conditions, we added an external impulse to the first operational amplifier in the first circuit for 1[s] approximately. The coupling is introduced through resistors $R_{9,10,11}$ and potentiometer R_{12} , which is a controlling device. Applying Kirchhoff's laws, it is possible to show that the circuit is described by Eqs (7) where $\alpha = \frac{1}{R_4 R_7 C_1 C_2}$, $\beta = \frac{0.01}{R_4 R_8 C_1 C_2}$, $k = \frac{1}{R_4 R_9 C_1 C_2}$, $\tau = \sqrt{\alpha t}$ and $b = -\frac{1}{R_1 C_1}$. In our experiment we used out of shelf elements; resistors $R_1, R_4, R_{10}, R_{11}, R_{12} = 10$ [k Ω], $R_2, R_3, R_5, R_6 = 100$ [k Ω], $R_7 = 100$ [k Ω], $R_8 = 1$ [k Ω], $R_9 = 10$ [k Ω] with tolerance $\pm 1\%$ and capacitors $C_1, C_2 = 10$ [μ F] with tolerance $\pm 10\%$. Symbols (a) and (b) in description of electrical elements in Figure 4(a) correspond to first and second system. An introduction of the resistor R_1 in scheme given by green connection causes appearance of negative damping in the circuit.

With this values of electrical elements we get following dimensionless parameters: $\alpha = 10$, $\beta = 10$, $k = 100$ and natural frequency $\omega_0 = \sqrt{\alpha}$. Such parameters let us slow down experimental circuit and store data with Multifunction Data Acquisition device (National Instruments USB-6259 BNC). In real experiment it is nearly impossible to build pure Hamiltonian system (the resistance of cables and capacitors is small but positive), so in case R_1 is absent the circuit is slightly damped and after sufficient time we observe converges of the trajectory to one of steady states. Nevertheless, this time is long enough to observe dynamics shown in numerical investigation in previous Section.

In Figure 5 we present comparison of experimental (a,b) and numerical (c,d) time traces of $x_1(t)$ for nearly Hamiltonian system with small positive damping (absence of R_1). After application of initial perturbation, system starts to behave chaotically (see zooms in Figure 5(b,d)), then we observe a slow decrease of amplitude. When $\tau = 320$ we see a transition from the chaotic motion to the quasiperiodic oscillations around one of the stable steady state. After long time (out of range of acquisition) circuit reaches equilibrium ($x_{10} = x_{30} = 1.0$, $x_{20} = x_{40} = 0.0$). For numerical calculation we take damping value $b = 0.0065$, which is small value (logarithmic decrement is equal to $\Delta = 1.67 \times 10^{-4}$). The experimental results are rescaled to dimensionless values.

In Fig. 6 we present Duffing oscillators with small negative damping. The damping in circuits (see 4(a)) is introduced by green connection with resistor $R_1 = 2.5$ [M Ω]. The negative damping firstly compensate the positive internal damping (always present in the system) and secondly pump energy to the system. Originally both Duffing systems are in equilibrium, then we perturb system similarly as in the case of positive damping. In Fig. 6 we present comparison of experimental (a,b) and numerical (c,d) time traces of $x_1(t)$. In numerical calculation we used $b = -0.01$. The evolution of system starts from chaotic behavior (see zooms in Fig. 6(b,d)) then amplitudes increase due to supply of energy by negative damping. For $\tau \approx 80$ we observe the

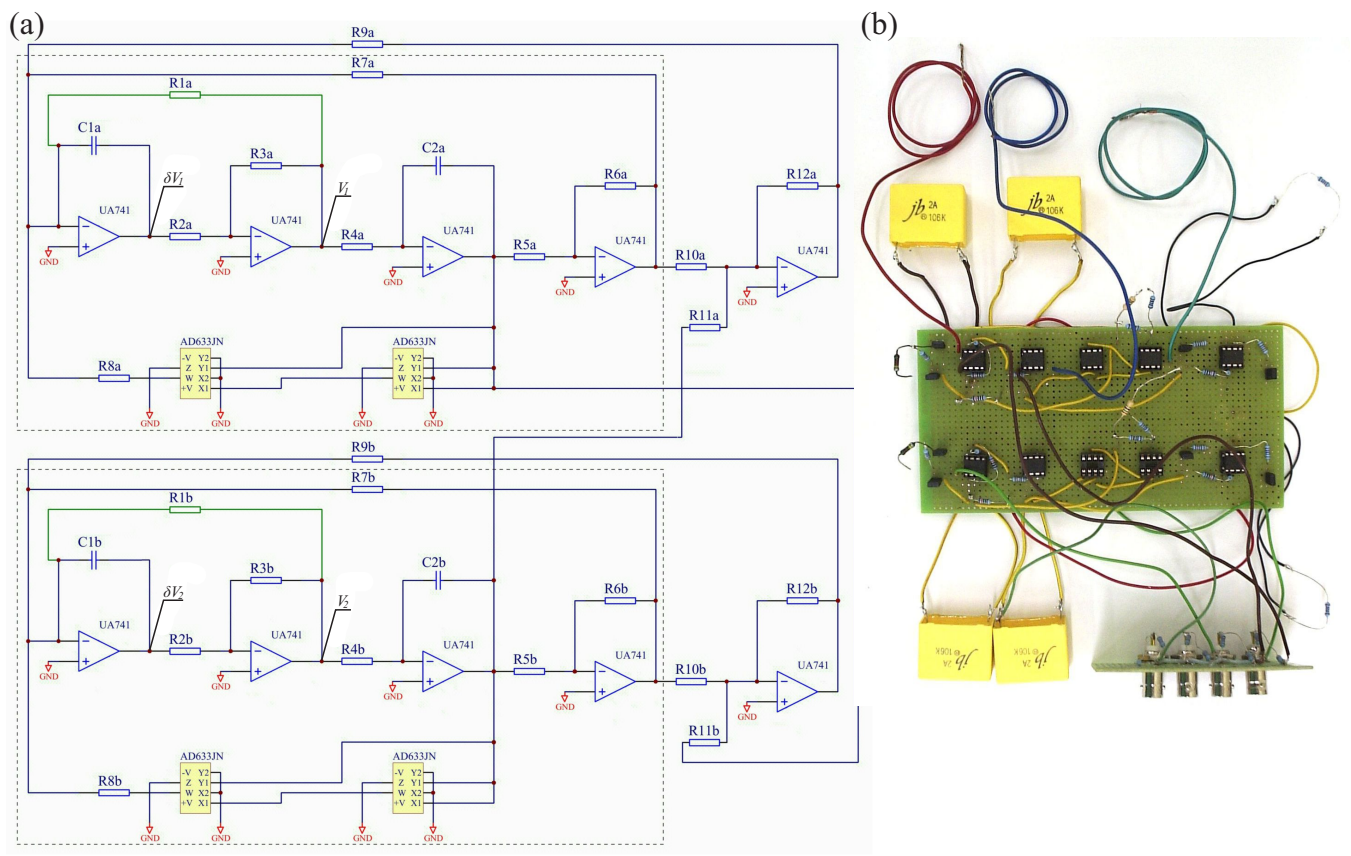


Figure 4: Scheme (a) and photo (b) of the analyzed of two coupled Duffing systems electrical realization .

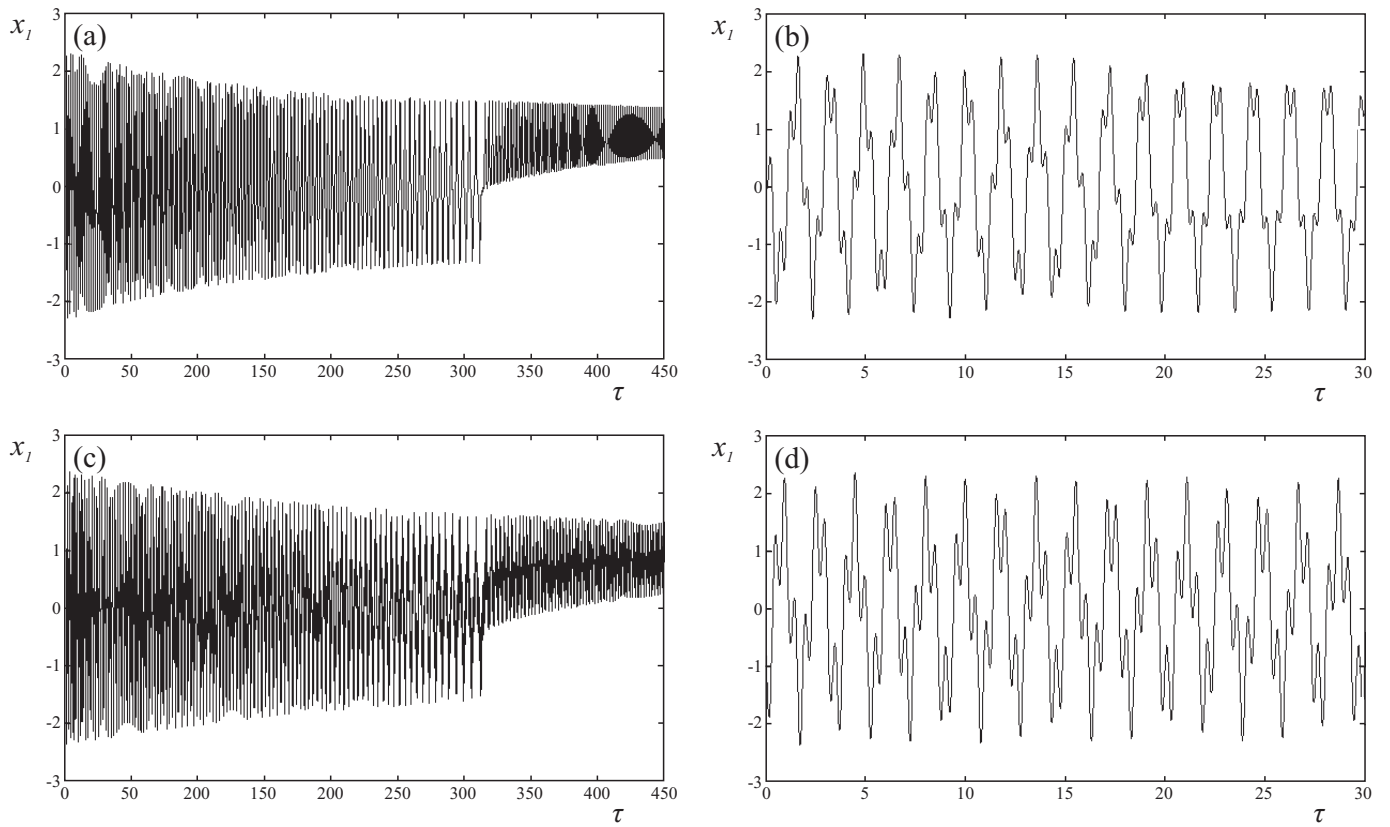


Figure 5: Time series $x_1(t)$ of nearly Hamiltonian system with positive damping (absence of R_1) in (a) experimental results and in (c) numerical results. In (b,d) zoom of chaotic motion from experiment and numeric respectively.

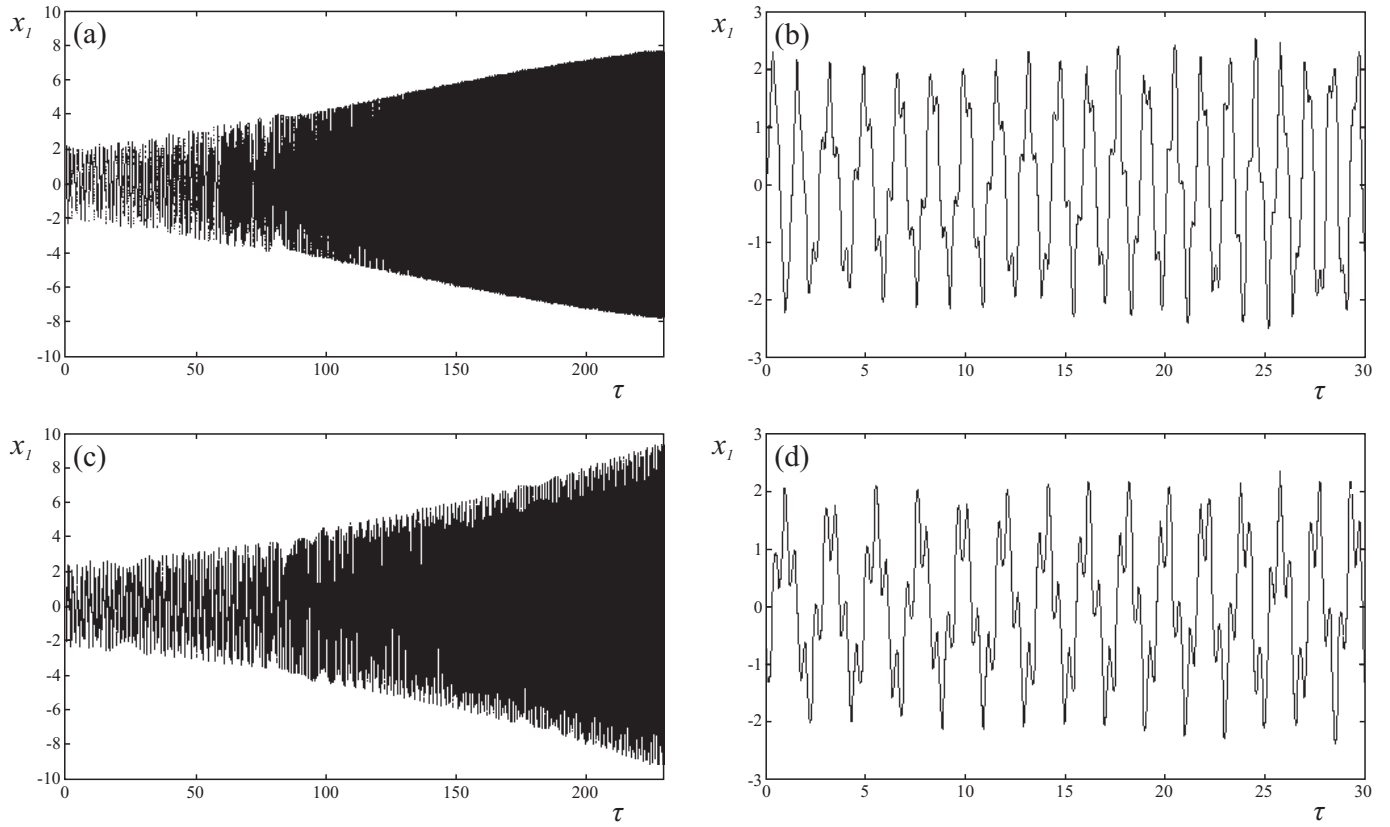


Figure 6: Time series $x_1(t)$ of nearly Hamiltonian system with negative damping ($R_1 = 2.5 [M\Omega]$) in (a) experimental results and in (c) numerical results. In (b,d) zoom of chaotic motion from experiment and numeric respectively.

transition to quasiperiodic motion. The voltage amplitude in experimental circuit cannot escape to infinity as trajectory in the case of numerical studies. The system is powered by a symmetric ± 15 [V] operational amplifiers, in our experimental setup we use amplifiers *LM358*. When one of the voltage amplitude reaches 13.8 [V] the saturation point of operational amplifiers is achieved. For this critical value signals are cut by operational amplifiers and the dynamics of the system is no more described by previously derived equations 7. In our case the signals $\delta V_{1,2}$ reach saturation for $\tau = 220$, hence we show system evolution up to this value. In theoretical studies of operational amplifiers one can find formula $|U_{Saturation}| = |0.9U_{Power}|$, which perfectly fit to our experimental results.

6. Conclusions

To summarize, this paper describes the dynamics of two coupled nearly Hamiltonian Duffing oscillators realized by electronic circuit. We investigate the properties of quasiperiodic and chaotic trajectories for different energy levels. We show that in the weakly perturbed near Hamiltonian system with small positive or negative damping the chaotic set in the phase space is not stable and is replaced by the chaotic saddle. The stable fixed points become attracting (positive damping) or repelling (negative damping) fixed points, and all KAM curves are destroyed and are replaced by unstable tori. Although transient chaotic motion generally exists, the phase trajectory tends to one of the fixed points or escapes to infinity. In the considered system we observe transient chaos both in the neighborhood of chaotic saddle and unstable tori in the wide range of system parameters both in the numerical simulations and the experiments using electronic circuit. The qualitative change in the time series of the transient Lyapunov exponents indicates the transition between two types of transient chaos. The complete destruction of persistent chaos when a weak dissipation is added to a near-integrable Hamiltonian system is typical and robust behavior.

Acknowledgment

This work has been supported by the Foundation for Polish Science, Team Programme – Project No TEAM/2010/5/5. K.T. is indebted to the Lodz University of Technology for hospitality.

- [1] Buskirk R. V. and Jefries C., Observation of chaotic dynamics of coupled nonlinear oscillators, *Phys. Rev. A* 31 (1985) 3332.
- [2] Strogatz S. H., Marcus C. M., Westervelt R. M., Mirollo R. E., Collective dynamics of coupled oscillators with random pinning, *Phys. D* 36 (1989) 23.
- [3] Pikovsky, A. S., Escape exponent for transient chaos and chaotic scattering in nonhyperbolic Hamiltonian systems, *J. Phys. A: Math. Gen.* 25 (1992) L477-L481.
- [4] Lieberman, M.A., and Tsang, K.Y., Transient Chaos in Dissipatively Perturbed, Near-Integrable Hamiltonian Systems, *Phys. Rev. Lett.* 55 (1985) 908-911.
- [5] Chirikov, B.V., Transient chaos in quantum and classical mechanics, *Found. of Phys.* 16 (1986) 39-49.
- [6] Lai, Y.-C., Tel, T., Transient chaos: Complex Dynamics on Finite-Time Scales, Springer, Berlin, 2011.
- [7] Grabner, M., Dirksen, R. T., Suda, N., Beam, K. G., The II-III loop of the skeletal muscle dihydropyridine receptor is responsible for the bi-directional coupling with the ryanodine receptor, *J. of Biol. Chem.* 274 (1999) 21913-21919.
- [8] di Bernardo, D. Signorini, M. G., A model of two nonlinear coupled oscillators for the study of heartbeat dynamics, *Int. J. Bifurcat. Chaos* 8 (1998) 1975-1985.
- [9] Marichal, R. L., González, E. J., Marichal, G. N., Hopf bifurcation stability in Hopfield neural networks, *Neural Networks* 36 (2012) 51-58.
- [10] Laucht, A., Villas-Bôas, J. M., Stobbe, S., Hauke, N., Hofbauer, F., Böhm, G., Finley, J. J., Mutual coupling of two semiconductor quantum dots via an optical nanocavity, *Phys. Rev. B* 82 (2010) 075305.
- [11] Mahler, Günter, and Rainer Wawer. "Quantum networks: dynamics of open nanostructures." *VLSI Design* 8.1-4 (1998): 191-196.
- [12] Chiuri, A., Greganti, C., Mazzola, L., Paternostro, M., Mataloni, P., Linear Optics Simulation of Quantum Non-Markovian Dynamics, *Scientific Reports* 2 (2012)
- [13] Muhammad, A., Saif, F., Engineering entanglement mechanically." *Phys. Lett. A* 376 (2012) 2608–2612.
- [14] Bindu, V., V. M. Nandakumaran, Numerical studies on bi-directionally coupled directly modulated semiconductor lasers, *Phys. Lett. A* 277 (2000) 345-351.
- [15] Raúl, V., Mirasso, C. R., Fischer, I., Simultaneous bidirectional message transmission in a chaos-based communication scheme, *Opt. Lett.* 32 (2007) 403-405.
- [16] Gyugyi, L., Schauder, C. D., Williams, S. L., Rietman, T. R., Torgerson, D. R., Edris, A., The unified power flow controller: a new approach to power transmission control, *IEEE Trans. Power Del.*, 10 (1995) 1085-1097.

- [17] Tel, T., On the organization of transient chaos: application to irregular scattering, *J. Phys. A: Math. Gen.* 22 (1989) L691-L697.
- [18] Hikiyama T., Torri K., Ueda Y., Quasi-periodic wave and its bifurcation in coupled magneto-elastic beam system, *Phys. Lett. A* 281 (2001) 155.
- [19] MacDonald, A. H. and Plischke, M., Study of the driven damped pendulum: Application to Josephson junctions and charge-density-wave systems, *Phys. Rev. B* 27 (1983) 201–211.
- [20] Srebro R., The Duffing oscillator: a model for the dynamics of the neuronal groups comprising the transient evoked potential, *Electroencephalogr. Clin. Neurophysiol.* , 96 (1995) 561–573.
- [21] Brennan, M.J. and Kovacic, I., *The Duffing Equation: Nonlinear Oscillators and their Behaviour*, Wiley, 2011.
- [22] S. Boccaletti, V. Latora, Y. Moreno, M. Chavez, D.-U. Hwang, *Complex networks: Structure and dynamics*, *Phys. Rep.* 424 (2009) 175-308.
- [23] Perlikowski, P., Yanchuk, S., Wolfrum, M., Stefanski, A., Mosiolek, P., and Kapitaniak, T., Routes to complex dynamics in a ring of unidirectionally coupled systems, *Chaos* 20 (2010) 013111.
- [24] Pazó, D., Noelia M., Pérez-Muñuzuri, V., Wave fronts and spatiotemporal chaos in an array of coupled Lorenz oscillators. *Phys. Rev. E* 63 (2001) 066206.
- [25] Naik, S., Hikiyama, T., Vu, H., Palacios, A., In, V., Longhini, P., Local bifurcations of synchronization in self-excited and forced unidirectionally coupled micromechanical resonators, *J. Sound Vibrat.* 331 (2011) 1127–1142.
- [26] Resmi, V. and Ambika, G. and Amritkar, R.E., General mechanism for amplitude death in coupled systems, *Phys. Rev. E* 84 (2011) 046212.
- [27] Perlikowski, P., Jagiello, B., Stefanski, A., Kapitaniak, T., Experimental observation of ragged synchronizability, *Phys. Rev. E* 78 (2008) 17203.
- [28] Munuzuri A. P., Perez-Munuzuri V., Gumez-Gestena M., Chua L. O., Perez-Villar V., Spatiotemporal structures in discretely-coupled arrays of nonlinear circuits: a review, *Int. J. Bifurcat. Chaos* 5 (1995) 17.
- [29] Paul Raj S., Rajasekar S. J., Murali K., Coexisting chaotic attractors, their basin of attractions and synchronization of chaos in two coupled Duffing oscillators, *Phys. Lett. A* 264 (1999) 283.
- [30] Vincent, U.E., and Kenfack, A., Synchronization and bifurcation structures in coupled periodically forced non-identical Duffing oscillators, *Phys. Scr.* 77 (2008) 045005.
- [31] Lücken, L., Yanchuk, S., Two-cluster bifurcations in systems of globally pulse-coupled oscillators, *Phys. D* 241 (2011) 350–359
- [32] Engel, G. S., Calhoun, T. R., Read, E. L., Ahn, T. K., Mančal, T., Cheng, Y. C., Fleming, G. R., Evidence for wavelike energy transfer through quantum coherence in photosynthetic systems, *Nature*, 446 (2007) 782-786.
- [33] Starosvetsky, Y., Hasan, M. A., Vakakis, A. F., Manevitch, L. I., Strongly Nonlinear Beat Phenomena and Energy Exchanges in Weakly Coupled Granular Chains on Elastic Foundations, *SIAM J. App. Math.* 72 (2012) 337-361.
- [34] Ota, Y., Ohba, I., The crossover from classical to quantum behavior in Duffing oscillator based on quantum state diffusion, *Pramana* 59 (2002) 409-412.
- [35] Yeon, K. H., Lee, K. K., Um, C. I., George, T. F., Pandey, L. N., Exact quantum theory of a time-dependent bound quadratic Hamiltonian system, *Phys. Rev. A*, 48 (1993) 2716.
- [36] Peano, V., Thorwart M., Dynamics of the quantum Duffing oscillator in the driving induced bistable regime, *Chem. Phys.* 322 (2006) 135–143.
- [37] Stoker J. J., *Nonlinear Vibrations in Mechanical and Electrical Systems*, Wiley, New York, 1992.
- [38] Skokos, Ch., The Lyapunov characteristic exponents and their computation, *Lect. Notes Phys.* 790 (2010) 63-135.